JVST B
Journal of Vacuum Science & Technology B

ARTICLE

avs.scitation.org/journal/jvb

Empirical modeling and Monte Carlo simulation of secondary electron yield reduction of laser drilled microporous gold surfaces

Cite as: J. Vac. Sci. Technol. B 38, 013801 (2020); doi: 10.1116/1.5130683
Submitted: 6 October 2019 · Accepted: 22 November 2019 ·
Published Online: 17 December 2019

Asif Iqbal,[1] Jonathan Ludwick,[2] Steven Fairchild,[3] Marc Cahay,[2] Daniel Gortat,[4] Martin Sparkes,[4] William O'Neill,[4] Tyson C. Back,[3] and Peng Zhang[1,a)]

AFFILIATIONS

[1]Department of Electrical and Computer Engineering, Michigan State University, East Lansing, Michigan 48824-1226
[2]Spintronics and Vacuum Nanoelectronics Laboratory, University of Cincinnati, Cincinnati, Ohio 45221
[3]Materials and Manufacturing Directorate, Air Force Research Laboratory, Wright Patterson Air Force Base, Dayton, Ohio 45433
[4]Institute for Manufacturing, University of Cambridge, 17 Charles Babbage Road, Cambridge CB3 0FS, United Kingdom

Note: This paper is part of the Conference Collection: 32nd IVNC and 12th IVESC conferences (2019 Joint Meeting).
a)Author to whom correspondence should be addressed: pz@egr.msu.edu

ABSTRACT

This work investigates secondary electron yield (SEY) mitigation from a metal surface with a microporous array fabricated using the laser drilling technique. We propose a general empirical model to fit the experimentally measured SEY of a flat gold surface for normal and oblique incidences of primary electrons. Using this empirical model, we develop a two-dimensional Monte Carlo (MC) simulation scheme to determine the effective SEY of a microporous array. It is found that the SEY from a porous surface is significantly reduced compared to that of the flat surface. By taking into account all the generations of secondary electrons inside a well, our MC results are found to be in very good agreement with the experimental data. The dependence of the SEY on the aspect ratio of the micropores and porosity of the surface is examined. A simple empirical formula has been proposed to evaluate the effective SEY of the gold microporous array for pores of arbitrary aspect ratios.

I. INTRODUCTION

Secondary electron emission (SEE) from solids has been of interest for decades as it is important for the understanding of electron beam–solid interaction,[1,2] as well as for building new devices and equipment, such as microchannel plates, electron multipliers, and electron microscopes.[3,4] SEE causes performance degradation in rf accelerators, microwave components, and satellite communication systems by introducing effects like electron cloud, electrostatic discharge,[5,6] and multipactor effect.[7–11] Therefore, it is desirable for a multitude of applications to reduce the secondary electron yield (SEY), which refers to the average number of emitted secondary electrons per incident primary electron on a surface. Selecting proper materials with low SEY, such as TiN,[12,13] for device fabrication or surface coating is one popular way to reduce SEY. Joy has provided[14] a large database of SEY data as a function of the impact energy of the primary electrons for many materials. However, it is of challenge to have suitable materials with low SEY, especially for long-term operation under extreme system requirements.[6]

Another approach to reduce the SEY is by using artificially roughened or porous surfaces, as the secondary electrons emitted inside the pores may be trapped through collisions with the side walls of the gaps or pores, which can yield a lower surface SEY. Although first demonstrated in the 1930s–1940s,[15–17] SEY reduction by artificially roughened surfaces was difficult to control precisely due to the limited surface engineering techniques available at that time. In recent years, modern surface engineering tools and techniques have enabled us to precisely tailor surface topographies at the micro- and nanoscales. Recently, SEY mitigation of roughened metal surfaces has been observed at millimeter,[18,19] micrometer,[20] and nanometer[21] scales. Analytical formulation[18,20]

and computational modeling[6,18] have been adopted to investigate the SEY of porous surfaces.

In this paper, we study the SEY from microporous gold surfaces manufactured by laser drilling techniques. Firstly, we propose an empirical model to fit the experimentally measured SEY of a flat gold surface for both normal and oblique incidences of primary electrons. We employ this empirical model into a simple two-dimensional (2D) Monte Carlo (MC) simulation scheme to estimate the SEY of microporous gold surfaces with various aspect ratios of the micropores and porosities of the surface. It is found that the SEY from a microporous surface is significantly reduced compared to that of the flat surface. We compare our MC results with both experimental measurements and an analytical model by Ye *et al.*[6] and Sattler *et al.*[20] We find that the analytical model,[20] which accounts for only the first generation of secondary electrons inside the well, cannot accurately predict the effective surface SEY of microporous surfaces over a wide range of aspect ratios. By taking into account all generations of secondary electrons inside a well, our MC results are found to be in very good agreement with the experimental data. We analyze the dependence of SEY on the aspect ratio of the micropores and porosity of the metal plate and construct a simple scaling for surfaces with micropores of arbitrary aspect ratios.

II. EXPERIMENTAL METHOD

A. Microporous surface fabrication

Micropores on stainless steel (304SS) surfaces were fabricated using laser drilling techniques at the University of Cambridge. Samples of 304SS were irradiated at normal incidence by a linearly polarized Amplitude Systems Satsuma ultrafast laser, wavelength of 1030 nm, 350 fs pulse duration, the beam quality factor (representing the degree of variation of a beam from an ideal Gaussian beam) of $M^2 < 1.1$, maximum output power of 5 W, raw beam diameter of 4.4 mm with 12.7 mm focal length lens, and effective spot diameter of 4.1 μm. The experiments were conducted in ambient air at 300 K with a $\lambda/4$ wave plate for circular polarization. N_2 was used as the shielding gas for the lens against the drilling debris. The laser was focused on the substrate via three-axis Aerotech stage. The number of pulses was controlled with a pulse synchronized output of the laser. The laser setup is illustrated in Fig. 1. The pulse duration and laser power were measured using an APE PulseCheck autocorrelator and a Coherent LM-3 power meter, respectively. The treatment time was 2 s/pore. Three samples with 4×4 mm porous arrays were produced. Acetone was used to clean/remove contaminants from the 304SS sample surface prior to laser processing. Ultrasonic bath in acetone for 30 min was used to remove the debris postprocessing.

The samples were then shipped from the University of Cambridge to the Air Force Research Laboratory Materials and Manufacturing Directorate (AFRL/RXAP). The SEY measurements on different flat regions of Au coated surfaces showed better consistency than the ones measured on 304SS surfaces. We attributed this better measurement consistency to Au being known as an inert material. For this reason, the 304SS samples were wiped with acetone and methanol, and then 100 nm of Au was sputter deposited on their surfaces. The film deposition rate during sputtering

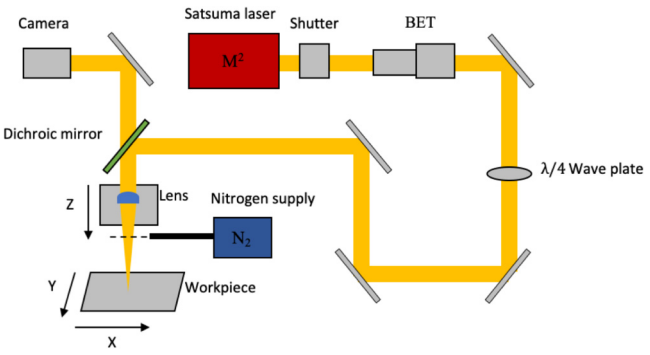

FIG. 1. Schematic of the experimental setup showing the Satsuma ultrafast laser, mechanical shutter, beam expander telescope (BET), $\lambda/4$ wave plate, dichroic mirror for inline beam monitoring, camera, focusing lens, three-axis motion stage, and nitrogen supply.

was monitored with a quartz crystal monitor to ensure accuracy of the film thickness; however, there is a possibility that the Au did not reach the inner surfaces of the pores. After the gold deposition, each sample was immediately loaded into the vacuum chamber for SEY measurements.

Veeco™ NT3300 white light interferometer was used for surface roughness measurements. For depth measurements of high aspect ratio holes, mechanical sectioning of the laser drilled holes was used. The cross-sectioned samples were polished, and the images were taken with an Olympus BX51™ optical microscope with a JENOPTIC™ ProgResC10+CCD camera. Hole diameter measurements were also recorded with the Olympus BX51™ optical microscope. For SEM images, Helios NanoLab DualBeam™ SEM was used. Figure 2(a) shows the optical image of the cross-sectioned sample 1, and Figs. 2(b) and 2(c) show the SEM images of sample 1 before gold sputtering. Table I records the characterization of the three produced samples after gold sputtering.

Aspect ratio of the micropores is defined as $A_R = H/2R$, where H is the hole depth and R is the hole radius. Porosity, ρ, is defined as the ratio of the pore surface area to the total surface area. The circularity of the hole is inferred from $C = 4\pi A/P^2$, where A is the area and P is the perimeter of the hole measured. For a circle, $C = 1$. The circularity of the produced holes was determined to be 0.97.

B. SEY measurements

The SEY measurements were carried out at AFRL/RXAP in an ultrahigh vacuum chamber sustaining a maximum pressure of 10^{-9} Torr. The primary electron beam was generated using an STAIB Instruments model DESA-150 analyzer with an integrated 0–5 keV electron gun that sustained a beam current of 20 nA in these measurements. The sample was mounted on a manipulation apparatus that allowed it to freely rotate in 360°. The measurements were then taken by following the two-step process as illustrated in Fig. 3.

In step 1, an electron beam impinges on the sample surface, allowing any generated secondary electrons from the sample to

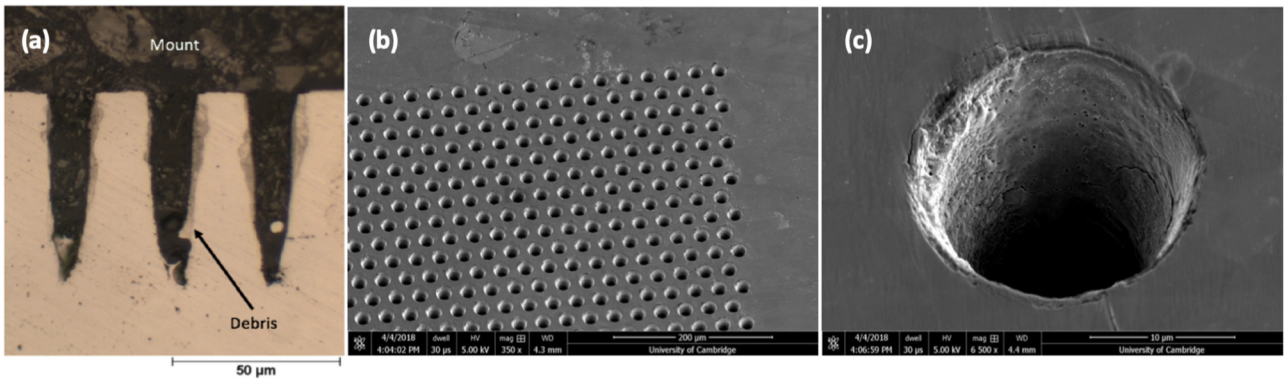

FIG. 2. (a) Optical image of cross-sectioned sample 1 before Au-coating. Debris present after mechanical sectioning and polishing. SEM images of the laser drilled surface of sample 1 with magnification (b) ×350 (c) ×6500.

freely emit. The net retained sample current is then measured (I_1). In step 2, a +100 V DC bias is applied to the sample. This forbids any generated secondary electrons with energies under 100 eV from emitting off the sample. The sample current is then measured again (I_2). The SEY (δ) can then be calculated using the following formula:

$$\delta = \frac{I_2 - I_1}{I_2}. \tag{1}$$

Each SEY measurement is an average of measurements taken at three separate arbitrary locations on both porous and flat regions of each sample to assess measurement reliability and to be able to assess the presence of spurious effects that would be linked to surface anomalies. At each location, the SEY was averaged over two measurements to ensure that any cathode instability or measurement error does not generate an erroneous data point. In the case of a large discrepancy between the two measurements, the data were removed and the SEY was remeasured.

The minimum beam diameter attainable by the electron source is 80 μm. Though this is too small to cover an adequate region of pores, the beam focus was adjusted to increase the beam size until SEY measurements were consistent across arbitrary pore region locations. This focus was then used for all measurements. The lowest porosity sample (sample 2) had a maximum SEY measurement standard deviation across all energies at five arbitrary location measurements of 0.0175, indicating the beam size was adequate.

Electron conditioning effects have been reported to lower a material inherent SEY[22] after electron beam exposure. To ensure this effect was negligible, each measurement location first collected SEY results over an initial energy sweep and then collected a second set of SEY results over another energy sweep at the same location. The SEY change from first and second sweeps was monitored. The peak SEY between these two sweeps averaged to be a 0.02 SEY change across all measurements, with a max peak SEY change of 0.05 SEY. This indicates that SEY errors from electron conditioning effects in this experiment can be considered negligible.

TABLE I. Characterization of the gold-coated laser drilled samples for SEY measurement.

Sample	Hole depth, H (μm)	Hole radius, R (μm)	Aspect ratio, $A_R = H/2R$	Porosity, ρ	Array type
1	60	9.9	3.02	0.40	Hexagonal
2	60	9.9	3.02	0.14	Hexagonal
3	60	8.5	3.52	0.50	Square

III. EMPIRICAL SEY MODEL

The empirical model and Monte Carlo simulation scheme were developed at Michigan State University. Our empirical model of SEY for flat surfaces is based on Vaughan's formula.[23–25] Vaughan's formula reads

$$\frac{\delta(\theta)}{\delta_{\max}(\theta)} = (we^{1-w})^k, \quad \text{for} \quad w \le 3.6, \tag{2a}$$

$$\frac{\delta(\theta)}{\delta_{\max}(\theta)} = 1.125/w^{0.35}, \quad \text{for} \quad w > 3.6, \tag{2b}$$

where $\delta(\theta)$ is the SEY for a primary electron of an impact angle θ with respect to the surface normal, $w = E_i/E_{\max}(\theta)$, with E_i being the impact energy of the primary electron, $k = 0.56$ for $w < 1$, and $k = 0.25$ for $1 \le w \le 3.6$. Here, $E_{\max}(\theta) = E_{\max 0}(1 + k_{sE}\theta^2/2\pi)$ and $\delta_{\max}(\theta) = \delta_{\max 0}(1 + k_{s\delta}\theta^2/2\pi)$, where k_{sE} and $k_{s\delta}$ are surface smoothness factors, $\delta_{\max 0}$ is the maximum value of δ at normal incidence, and $E_{\max 0}$ is the impact energy that yields $\delta_{\max 0}$ at normal incidence (i.e., $\theta = 0$).

Our model includes angle-dependent parameters to obtain good fitting to the experimental data, given by the following

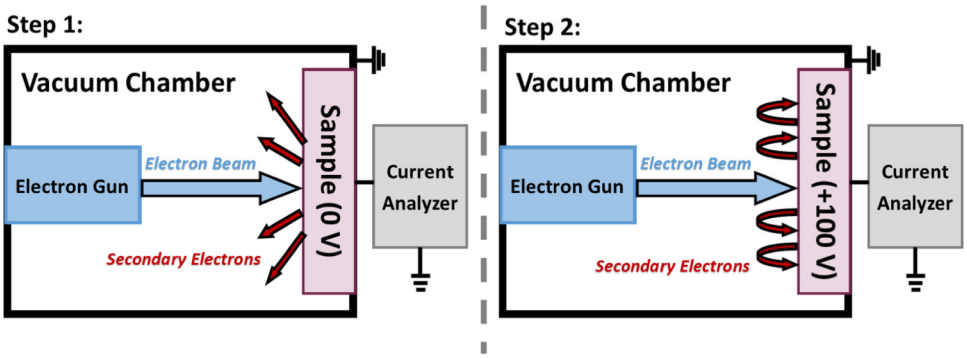

FIG. 3. Diagram of the SEY measurement system.

empirical equations:

$$\frac{\delta(\theta)}{\delta_{\max}(\theta)} = (we^{1-w})^k, \quad \text{for} \quad w \le 4.28, \tag{3a}$$

$$\frac{\delta(\theta)}{\delta_{\max}(\theta)} = c/w^d, \quad \text{for} \quad w > 4.28, \tag{3b}$$

where the angle-dependent parameters $E_{\max}(\theta)$ and $\delta_{\max}(\theta)$ are given by

$$E_{\max}(\theta) = E_{\max 0}(1 + k_{sE1}\theta + k_{sE2}\theta^2 + k_{sE3}\theta^3 + k_{sE4}\theta^4), \tag{4a}$$

$$\delta_{\max}(\theta) = \delta_{\max 0}(1 + k_{s\delta}\theta^2/2\pi), \tag{4b}$$

where $E_{\max 0}$ and $\delta_{\max 0}$ are the parameters for normal incidence (i.e., $\theta = 0$) and k_{sE1}, k_{sE2}, k_{sE3}, k_{sE4}, and $k_{s\delta}$ are fitting constants. For gold surfaces used in this work, the adopted empirical values for the parameters of Eq. (4) are $E_{\max 0} = 0.7$ KV, $\delta_{\max 0} = 1.6$, $k_{sE1} = -6.85$, $k_{sE2} = 26.76$, $k_{sE3} = -32.26$, $k_{sE4} = 12.65$, and $k_{s\delta} = 1.8$. The parameter k in Eq. (3a) is given by

$$k = a_0\left(1 + \frac{k_a\theta^2}{2\pi}\right), \quad \text{for} \quad w \le 1, \tag{5a}$$

$$k = b_0\left(1 + \frac{k_b\theta^2}{2\pi}\right), \quad \text{for} \quad 1 < w \le 4.28, \tag{5b}$$

and the parameters c and d in Eq. (3b) are, respectively, given by

$$c = c_0\left(1 + \frac{k_c\theta^2}{2\pi}\right), \tag{6a}$$

$$d = d_0\left(1 + \frac{k_d\theta^2}{2\pi}\right). \tag{6b}$$

The adopted values of the fitting coefficients in Eqs. (5) and (6) for the gold surfaces in this work are $a_0 = 0.76$, $k_a = -3$, $b_0 = 0.12$, $k_b = -2$, $c_0 = 1.375$, $k_c = 0.8$, $d_0 = 0.35$, and $k_d = 0.5$. Note that the proposed SEY model in Eqs. (3)–(6) is general and is expected to be able to fit virtually any SEY measurement data. It is also noteworthy that neither Vaughan's model nor our empirical model is based on the theoretical background. Both models are parameterizations of experimental curves.

IV. TWO-DIMENSIONAL MONTE CARLO MODEL

For simplicity, we model 3D cylindrical pores as 2D rectangular wells in our simulation scheme, by setting the width of the rectangular well D to be the same as the diameter $2R$ of the cylindrical pore, $D = 2R$, as shown in Fig. 4. Following Refs. 6 and 20, we calculate the effective SEY, δ_p, of a rectangular well by Monte Carlo (MC) simulation and then obtain the effective SEY of the porous surface, δ_{surf}, using this simulated value of δ_p. We start our simulation by considering $N_0 = 10^4$ particles normally incident at random locations on the bottom surface of a rectangular well of height H and width D [Fig. 4(b)] with a given impact energy E_i. Any kth particle initially carries $n_{0,k} = 1$ electron. From the empirical model for flat surfaces described above in Eqs. (3)–(6), we calculate the secondary electron yield $\delta_{1,k}$ for each of the primary impacts generating the first generation of secondary particles [Fig. 5(a)], each carrying $n_{1,k} = n_{0,k}\delta_{1,k}$ electrons. The emission

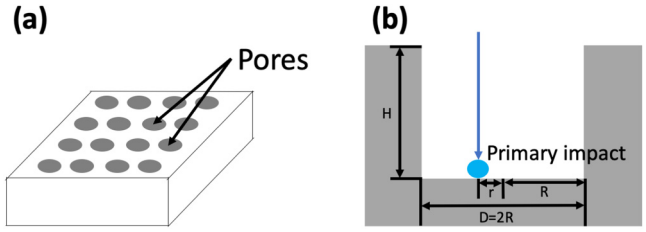

FIG. 4. (a) Schematic of a microporous surface geometry with 3D cylindrical pores. (b) The 2D rectangular well geometry assumed in our Monte Carlo model.

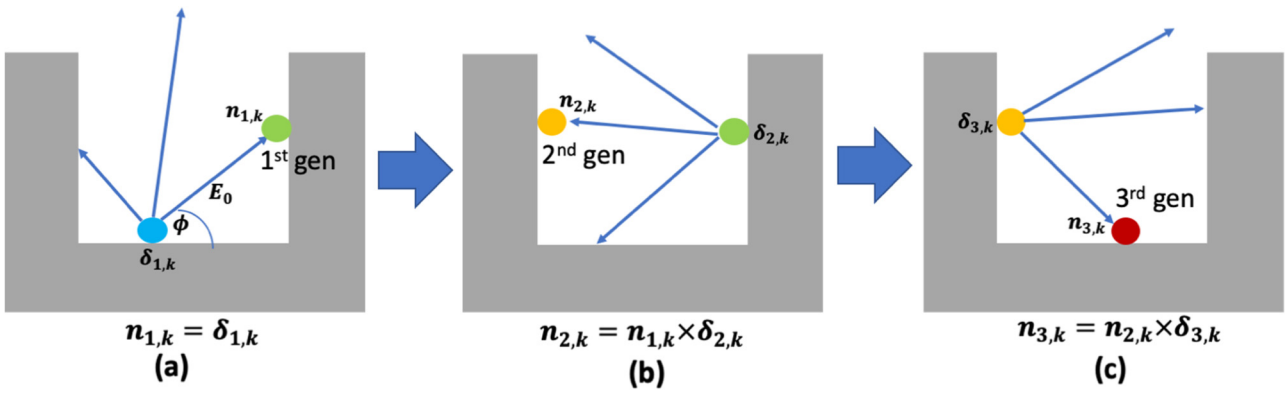

FIG. 5. 2D Monte Carlo simulation scheme. Each secondary particle generated inside the well can either escape the well or impact the inner walls of the well emitting the next generation of secondary particle. (a) A representative first generation of secondary particle is shown impacting the right wall. (b) A representative second generation of secondary particle is shown impacting the left wall. (c) A representative third generation of secondary particle is shown impacting the bottom wall. The total number of electrons contained in the ith generation of the kth particle is calculated as $n_{i,k} = n_{i-1,k}\delta_{i,k} = n_{0,k}\delta_{i,k}\delta_{i-1,k} \ldots \delta_{1,k}$.

energy E_0 and emission angle ϕ of the secondary particles are assigned according to the following distributions:[8,9]

$$f(E_0) = \frac{E_0}{E_{0m}^2} e^{-\frac{E_0}{E_{0m}}}, \tag{7}$$

$$g(\phi) = \frac{1}{2}\sin\phi, \tag{8}$$

where $E_{0m} = 0.005E_{\max 0}$ is the peak of the distribution of emission energies with the expectation value of $E_0 = 2E_{0m}$. Note that one limitation of using Eq. (7) is that the energy of an emitted secondary particle is independent of the energy of the impacting primary particle.

Some of these first generation secondaries escape the well. The rest impact the side walls of the well and generate the second generation of secondaries [Fig. 5(b)]. These, in turn, either escape the well or impact the inner surfaces of the well again, emitting the third generation of secondaries [Fig. 2(c)]. The total number of electrons contained in the ith generation of the kth particle is calculated as $n_{i,k} = n_{0,k}\delta_{i,k}\delta_{i-1,k} \ldots \delta_{1,k}$. If $n_{i,k} < 0.001$, we consider that the particle is absorbed by the wall at the ith impact. We keep tracking the particles inside the well until all the particles either escape the well or are absorbed by the inner surfaces. The total number of escaping electrons N_e is recorded at the end of the simulation. The average effective SEY from the rectangular well is then calculated as $\delta_p = N_e/N_0$. The SEY for a flat surface δ_f is given as in Eq. (3), which is also able to be recovered from the MC simulation. The effective SEY of a porous surface is then obtained as[6,20]

$$\delta_{\text{surf}} = \delta_p\rho + \delta_f(1-\rho), \tag{9}$$

where ρ is the porosity, which is defined as the ratio of the pore surface area to the total surface area. The SEY model parameters for the flat region, the bottom surface, and the side walls of the wells are assumed to be the same.

V. RESULTS

Figure 6 shows the comparison of the predicted SEY curves from the proposed empirical SEY model in Eq. (3) (blue lines) and Vaughan's SEY model in Eq. (2) (red lines) with the experimentally measured SEY curves (black lines) for flat gold surfaces for incident angles of $\theta = 0°$, 15°, 60°, and 75°. As shown in Fig. 6, it is clear that Vaughan's model underestimates the experimental results, especially when the impact energy is larger than 1 kV. Vaughan's model is not able to accurately predict the angular sensitivity of the experimental measurements of SEY either. Our empirical model, Eq. (3), overcomes these limitations with the inclusion of proper angle-dependent parameters and fit the experimental measurements very accurately, as shown in Fig. 6.

Figure 7 shows the comparison of the predicted two-dimensional SEY curves from the analytical model proposed by Ye *et al.* [Eq. (4) in Ref. 6] and Sattler *et al.* [Eqs. (1), (2), and (7) in Ref. 20] (red lines), and our MC simulation results (blue lines) with the measured SEY curves (black lines) for normal incidence of primary electrons on three different samples of microporous gold surfaces with different aspect ratio $A_R = H/D$ of the pores and porosity ρ of the surface. It is clear from Fig. 7 that the SEY from a porous surface [Figs. 7(b)–7(d)] is significantly lower than that from a flat surface [Fig. 7(a)]. The lowest SEY (peak value of 1.266 compared to 1.605 of the flat surface) is obtained for the sample 3 [Fig. 7(d)], which has the maximum porosity of the surface $\rho = 0.50$ and the maximum aspect ratio $A_R = 3.52$. A previous study has shown that the Ye-Sattler's analytical model agrees well with the measured SEY for surfaces with micropores of small aspect ratio ($A_R < 0.55$).[20] However, as evident from Fig. 7, the analytical model

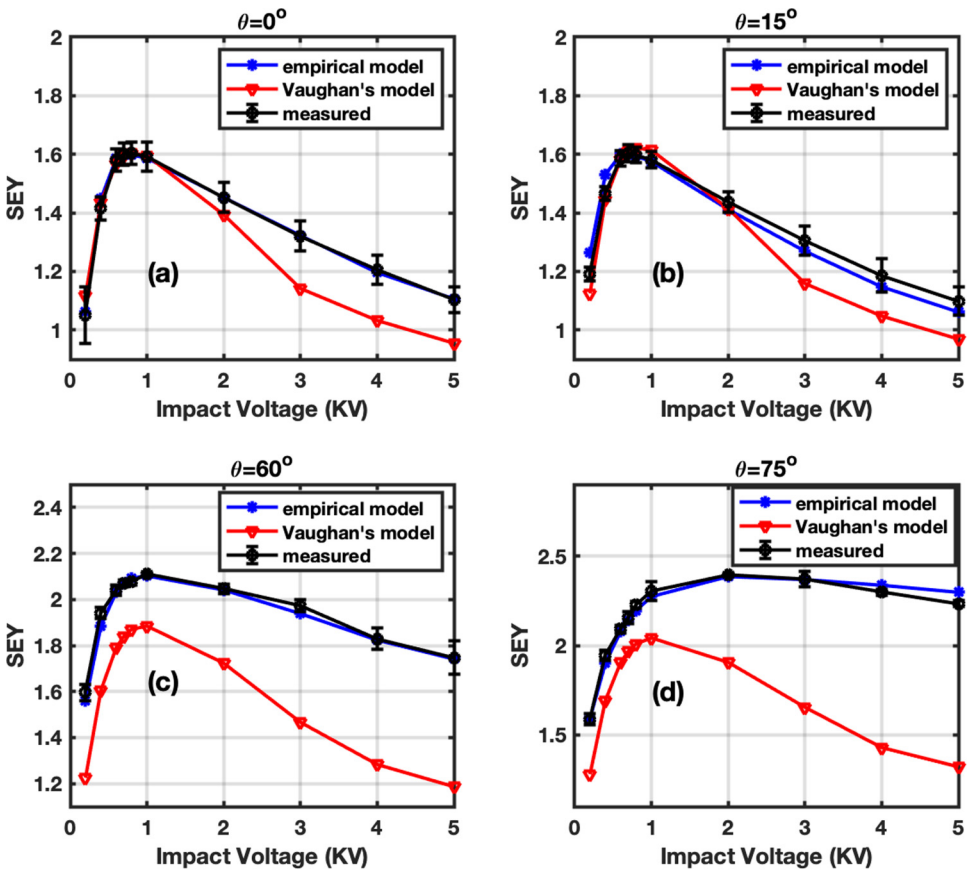

FIG. 6. Comparison of the predicted SEY curves from the proposed empirical SEY model, Eq. (3) (blue lines), and Vaughan's SEY model of Eq. (2) (red lines) with the measured SEY curves (black lines) for flat gold surfaces for incident angles of (a) $\theta = 0°$, (b) $\theta = 15°$, (c) $\theta = 60°$, and (d) $\theta = 75°$. Error bars represent a 95% confidence interval of the experimental data. We set $k_{sE} = k_{s\delta} = 1$ for Vaughan's model in Eq. (2). The predicted curve from the proposed empirical SEY model (blue line) in Fig. 6(a) is overlaid with the measured SEY curve (black line).

underestimates the effective surface SEY for micropores with a large aspect ratio ($A_R > 3$). This is attributed to the fact that the analytical model accounts only for the first generation of secondary electrons generated inside the well, which is a good approximation for small aspect ratio micropores. For small aspect ratio micropores, most of the first generation of secondary electrons escape the well and only a small portion of them get trapped inside the well and generate the subsequent generations of secondaries. Our MC results take into account all the subsequent generations of secondary electrons generated inside the well, which are in very good agreement with the experimental measurements, as shown in Fig. 7. This indicates that the subsequent generations of secondary electrons inside the well contribute significantly to the effective SEY of a porous surface for relatively large aspect ratio of micropores. The slight overestimation of the simulation results, especially for impact voltage larger than 1 kV, is due to the fact that the simulation uses a simplified 2D model, whereas the experimental measurements were conducted on surfaces with 3D cylindrical pores. In addition, the geometry of the micropores in the experimental samples is not ideally cylindrical, but with tapered bottom [Fig. 2(a)], which may give a different SEY than the ideal geometries used in the simulation.

Figure 8 shows the dependence of a microporous surface SEY on the aspect ratio of the micropores for the porosity of the surface, $\rho = 0.40$ and 0.50, with different incident energies of electrons $E_i = 0.4\,\text{kV}$, $0.7\,\text{kV}$, $1\,\text{kV}$, and $3\,\text{kV}$ from our MC simulations. It is evident from Figs. 8(a)–8(d) that with the increase of the aspect ratio A_R of the micropores, the effective SEY of the surface decreases sharply when $A_R < 10$, then decreases slowly when $A_R > 10$, and gradually approaches an asymptotic minimum value as A_R further increases. This observation is important as it implies that an optimum aspect ratio may be obtained for specific requirements in various applications.

Based on the MC simulations, we extend the analytical formula of effective SEY from shallow pores[6,20] to be with an arbitrary aspect ratio A_R,

$$\delta_{p,\text{effective}} = \sigma + C_1[\cos(\tan^{-1}(C_2A_R + C_3A_R^2)) + \cos(\tan^{-1}(C_4A_R + C_5A_R^2))], \tag{10}$$

where σ is the backscattering coefficient and C_1, C_2, C_3, C_4, and C_5 are fitting coefficients. Putting Eq. (10) into Eq. (9), we obtain the following formula for calculating the effective SEY for surfaces with

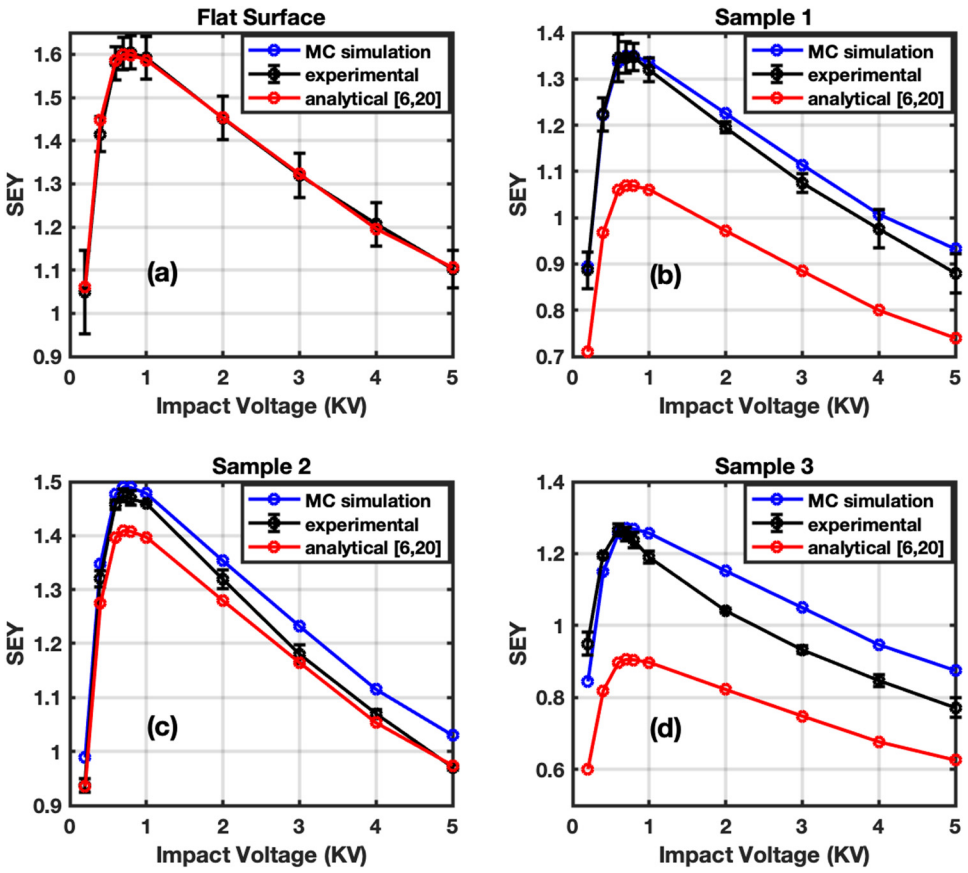

FIG. 7. Comparison of the predicted SEY curves from the analytical model (Refs. 6 and 20) (red lines) and our MC simulation results (blue lines) with the measured SEY curves (black lines) for normal incidence of primary electrons on four different samples of the microporous gold surface with different aspect ratio of the pores, A_R, and surface porosity, ρ: (a) flat surface sample with $A_R = 0$, $\rho = 0$, (b) sample 1 with $A_R = 3.02$, $\rho = 0.40$, (c) sample 2 with $A_R = 3.02$, $\rho = 0.14$, and (d) sample 3 with $A_R = 3.52$, $\rho = 0.50$. Error bars represent a 95% confidence interval of the measured data. The predicted SEY curve from the Monte Carlo simulation (blue line) and the measured SEY curve (black line) in Fig. 7(a) are overlaid with the predicted SEY curve from the analytical model (red line).

arbitrary porosity ρ:

$$\delta_{\text{surf,effective}} = \delta_{p,\text{effective}}\rho + \delta_f(1-\rho). \tag{11}$$

Since $\delta_{p,\text{effective}} = \delta_f$ for $A_R = 0$, we have from Eq. (10), $C_1 = (\delta_f - \sigma)/2$. To obtain a good fitting quality for the gold samples, we choose $\sigma = 0.03$, $C_2 = 2.0$, $C_3 = -0.012$, $C_4 = 0.2$, and $C_5 = 0.0065$. Figure 8 shows that the effective SEY values obtained from the empirical Eq. (11) (dotted lines) are in excellent agreement with the MC simulation results (solid lines) for porosities $\rho = 0.40$ and $\rho = 0.50$. It is also clear from Figs. 8(a)–8(d) that the analytical model[20] (dashed lines) that accounts for only the first generation of secondary electrons inside the well underestimates the effective SEY of the surfaces for $A_R < 40$. However, as A_R increases, the effective surface SEY obtained from the MC simulations, the analytical model, and the empirical Eq. (11) approaches the same asymptotic minimum value $\delta^{\min}_{\text{surf, effective}} = \sigma\rho + \delta_f(1-\rho)$ as $A_R \to \infty$. Figures 8(e)–8(h) show the zoomed plots of Figs. 8(a)–8(d) in the range of aspect ratio, $0 \le A_R \le 4$. From these plots, we can see that the difference between the MC simulation results (solid lines) and the analytical model of Ref. 20 (dashed lines) is less prominent in the range $0 \le A_R \le 0.25$. We conclude from the above discussion that the multigenerations of the secondary electrons generated inside the well are most important in the range of the aspect ratio, $0.25 < A_R < 40$, where the simple analytical model by Ye *et al.* [Eq. (4) in Ref. 6] and Sattler *et al.* [Eqs. (1), (2), and (7) in Ref. 20] will become unreliable. Instead, our empirical model, Eqs. (10) and (11), gives a good approximation over the entire range of A_R.

To understand the dependence of the effective SEY of the microporous surface on the surface porosity, we can recast Eq. (11) as

$$\begin{aligned}\delta_{\text{surf,effective}} &= \delta_{p,\text{effective}}\rho + \delta_f(1-\rho)\\ &= (\delta_{p,\text{effective}} - \delta_f)\rho + \delta_f.\end{aligned} \tag{12}$$

It is clear from the above equation that the effective SEY of the microporous surface depends linearly on the porosity of the surface. The SEY decreases with surface porosity only if $\delta_{p,\text{effective}} < \delta_f$. In the case of $\delta_{p,\text{effective}} > \delta_f$, which, for example, may occur with appropriate surface coating, the SEY increases with the surface porosity. Therefore, for the purpose of SEY reduction, the microporous surfaces need to be carefully designed with a sufficiently reduced SEY for the pores.

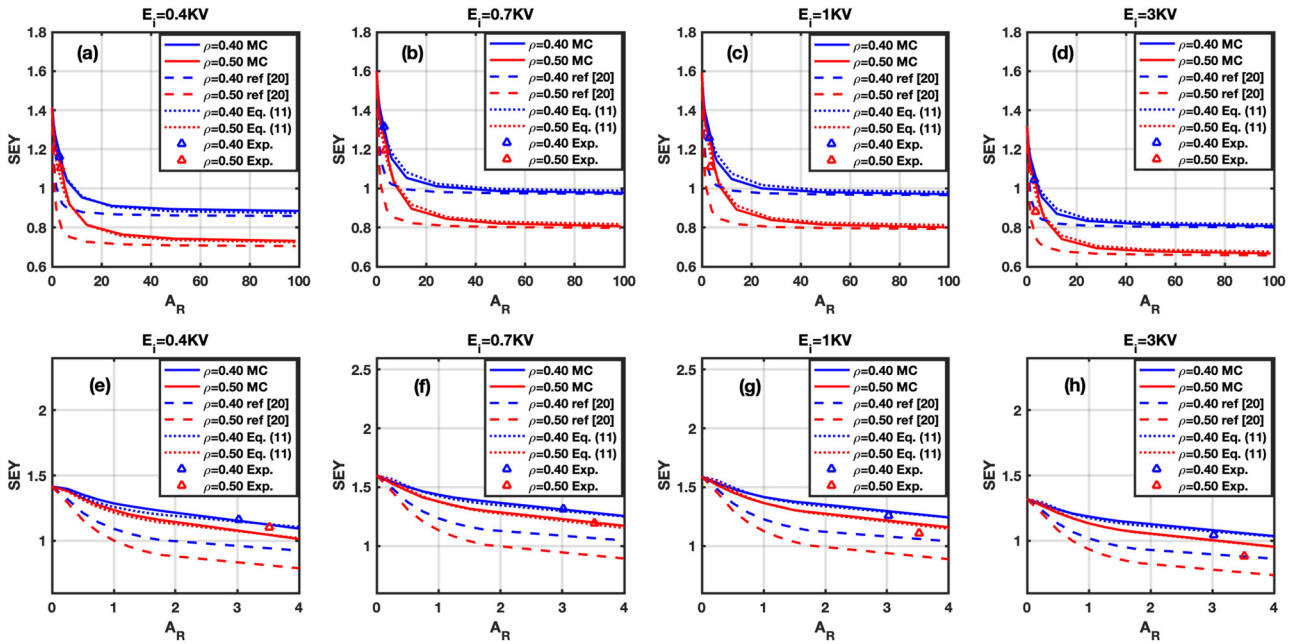

FIG. 8. Effective surface SEY vs aspect ratio of the micropores, A_R, for surface porosities, $\rho = 0.40$ (blue lines) and $\rho = 0.50$ (red lines) from Monte Carlo simulations (solid lines), analytical model (Ref. 20) (dashed lines), empirical Eq. (11) (dotted lines), and experimental data (triangles) for different incident energies of electrons; Top row: (a) $E_i = 0.4$ kV, (b) $E_i = 0.7$ kV, (c) $E_i = 1$ kV, (d) $E_i = 3$ kV in the large range of the aspect ratio, $0 \leq A_R \leq 100$. Bottom row: (e)–(h) enlarged view in the range of the aspect ratio, $0 \leq A_R \leq 4$, for (a)–(d), respectively.

VI. CONCLUDING REMARKS

In this work, an empirical model has been proposed to fit the experimentally measured SEY of flat gold surfaces for both normal and oblique incidences of primary electrons. A 2D Monte Carlo simulation scheme has been employed using this empirical SEY model to investigate the SEY mitigation from gold surfaces with microporous arrays prepared using a laser drilling technique. Three microporous array samples with different array types, aspect ratio of micropores, and porosity of the surface are tested. Compared to the flat surface, the SEYs from all the three microporous surfaces are reduced. The most effective SEY reduction (peak value of 1.266 compared to 1.605 of the flat surface) is achieved for the sample with the maximum surface porosity $\rho = 0.50$ and the maximum aspect ratio of micropores $A_R = 3.52$. By taking into account all the generations of secondary electrons generated inside a 2D rectangular well, our MC simulation results are found to be in very good agreement with the experimental data. The dependence of SEY reduction on the aspect ratio of the micropores and the porosity of the surface are examined in detail. An empirical formula has been proposed to estimate the effective SEY of a microporous array for arbitrarily given surface porosity and aspect ratio of the micropores.

Future works may include studies of SEY for oblique incidence of primary electrons on microporous array surface structures. A more accurate simulation model may be developed to account for the three-dimensional geometry of pores. Different pore geometries may be explored. The effects of energy loss during multigenerations of secondary electron emission as well as the energy and angular distributions of the resulted secondary electrons are also subjects of future research. It would also be of interest to explore the possible application of our SEY modeling for micropores of very large aspect ratios to carbon nanotube forests[4,26,27] or materials of similar morphology. Another important future study is to evaluate the effects of surfaces with microporous holes on the operation of RF or microwave devices, e.g., superconducting RF guns,[28] and depressed collectors in traveling wave tubes.[29]

ACKNOWLEDGMENTS

The work was supported by the Air Force Office of Scientific Research under Award Nos. FA9550-18-1-0061 and FA9550-18-1-0062 and by the Air Force Office of Scientific Research under Award No. FA9550-17RXCOR428. A.I. also gratefully acknowledges the MIPSE Graduate Fellowship. J. Ludwick received funding from the State of Ohio through the Dayton Area Graduate Studies Institute (DAGSI) program, Contract No. FA8650-12-2-7248 (R22021, Topic No.: RX15-10).

REFERENCES

[1]E. M. Baroody, Phys. Rev. **78**, 780 (1950).
[2]A. J. Dekker, in *Solid State Physics*, edited by F. Seitz and D. Turnbull (Academic Press, Cambridge, MA, 1958), pp. 251–311.

[3]S. Pendyala and J. W. McGowan, Can. J. Phys. **52**, 2215 (1974).
[4]M. K. Alam, P. Yaghoobi, and A. Nojeh, Scanning **31**, 221 (2009).
[5]M. Furman and M. Pivi, Phys. Rev. Spec. Top. Accel. Beams **5**, 124404 (2002).
[6]M. Ye, Y. N. He, S. G. Hu, R. Wang, T. C. Hu, J. Yang, and W. Z. Cui, J. Appl. Phys. **113**, 074904 (2013).
[7]J. R. M. Vaughan, IEEE Trans. Electron Devices **35**, 1172 (1988).
[8]R. A. Kishek and Y. Y. Lau, Phys. Rev. Lett. **80**, 193 (1998).
[9]P. Zhang, Y. Y. Lau, M. Franzi, and R. M. Gilgenbach, Phys. Plasmas **18**, 053508 (2011).
[10]A. Iqbal, J. Verboncoeur, and P. Zhang, Phys. Plasmas **25**, 043501 (2018).
[11]A. Iqbal, J. Verboncoeur, and P. Zhang, Phys. Plasmas **26**, 024503 (2019).
[12]I. Montero, S. H. Mohamed, M. García, L. Galán, and D. Raboso, J. Appl. Phys. **101**, 113306 (2007).
[13]A. Ruiz, E. Román, P. Lozano, M. García, L. Galán, I. Montero, and D. Raboso, Vacuum **81**, 1493 (2007).
[14]D. C. Joy, "A database of electron-solid interactions," Revision # 08-1, 2008. See: http://web.utk.edu/~srcutk/htm/interact.htm.
[15]H. Bruining, J. H. De Boer, and W. G. Burgers, Physica **4**, 267 (1937).
[16]H. Bruining, Philips Tech. Rev. **3**, 80 (1938); available at https://www.americanradiohistory.com/Archive-Philips-Technical-Review/30s/Philips-Technical-Review-1938.pdf.
[17]J. L. H. Jonker, Philips Tech. Rev. **3**, 211 (1938); available at https://www.americanradiohistory.com/Archive-Philips-Technical-Review/30s/Philips-Technical-Review-1938.pdf.
[18]M. Pivi, F. K. King, R. E. Kirby, T. O. Raubenheimer, G. Stupakov, and F. Le Pimpec, J. Appl. Phys. **104**, 104904 (2008).
[19]C. Watts, M. Gilmore, and E. Schamiloglu, IEEE Trans. Plasma Sci. **39**, 836 (2011).
[20]J. M. Sattler, R. A. Coutu, R. Lake, T. Laurvick, T. Back, and S. Fairchild, J. Appl. Phys. **122**, 055304 (2017).
[21]V. C. Nistor *et al.*, "New coatings of silver and gold with strong surface roughness for significantly reducing multipactor effect in RF components," in *6th International Workshop on Multipactor, Corona and Passive Intermodulation*, Valencia, Spain, September 2008.
[22]R. Valizadeh, O. B. Malyshev, S. Wang, S. A. Zolotovskaya, W. Allan Gillespie, and A. Abdolvand, Appl. Phys. Lett. **105**, 231605 (2014).
[23]R. M. Vaughan, IEEE Trans. Electron Devices **40**, 830 (1993).
[24]J. R. M. Vaughan, IEEE Trans. Electron Devices **36**, 1963 (1989).
[25]J. Ludwick, G. Tripathi, M. Cahay, S. B. Fairchild, P. T. Murray, and T. C. Back, AIP Adv. **8**, 085017 (2018).
[26]B. Wood, J. Lee, G. Wilson, T. Shen, and J. R. Dennison, IEEE Trans. Plasma Sci. **47**, 3801 (2019).
[27]M. K. Alam, P. Yaghoobi, and A. Nojeh, J. Vac. Sci. Technol. B **28**, C6J13 (2010).
[28]E. T. Tulu, U. van Rienen, and A. Arnold, Phys. Rev. Accel. Beams **21**, 113402 (2018).
[29]J. Wang, Y. Gao, Z. You, J. Fan, J. Zhang, S. Wang, and Z. Xu, Appl. Sci. **9**, 4374 (2019).